Int J Earth Sci (Geol Rundsch) (2017) 106:2171–2188
DOI 10.1007/s00531-016-1421-1

ORIGINAL PAPER

Gas accumulations in Oligocene–Miocene reservoirs in the Alpine Foreland Basin (Austria): evidence for gas mixing and gas degradation

L. Pytlak[1] · D. Gross[1] · R. F. Sachsenhofer[1] · A. Bechtel[1] · H.-G. Linzer[2]

Received: 17 February 2016 / Accepted: 3 November 2016 / Published online: 19 November 2016

Abstract Two petroleum systems are present in the eastern (Austrian) sector of the Alpine Foreland Basin. Whereas oil and thermogenic gas in Mesozoic and Eocene reservoir rocks have been generated beneath the Alps in Lower Oligocene source rocks, relative dry gas in Oligocene–Miocene clastic rocks deposited in the deep marine basin-axial channel system (Puchkirchen Channel) is interpreted as microbial in origin. Detailed investigations of the molecular and isotope composition of 87 gas samples from 86 wells, representing all producing fields with Oligocene and Miocene reservoir rocks, suggest that the presence of pure microbial gas is rare and limited mainly to the northern basin flank (e.g., KK field). All other fields contain varying amounts of thermogenic gas, which has been generated from a source rock with oil-window maturity. A relation with the underlying thermogenic petroleum system is obvious. Upward migration occurred along discrete fault zones (e.g., H field) or through low-permeability caprocks. Local erosion of Lower Oligocene sediments, the principal seal for the thermogenic petroleum system, as well as a high percentage of permeable rocks within the Puchkirchen Channel favored upward migration and mixing of thermogenic and microbial gas. All gas samples in Oligocene–Miocene reservoirs are biodegraded. Biodegradation and the formation of secondary microbial gas resulted in gas drying. Therefore, the gas samples analyzed in this study are relative dry, despite significant contributions of thermogenic hydrocarbons. Biodegradation probably continues at present time. The degree of biodegradation, however, decreases with depth.

Keywords Foreland basin · Gas mixing · Gas biodegradation · Secondary microbial methane

✉ L. Pytlak
Lukasz.Pytlak@onet.pl; Lukasz.Pytlak@unileoben.ac.at

[1] Department Applied Geosciences and Geophysics, Chair of Petroleum Geology, Montanuniversitaet, Peter-Tunner-Strasse 5, 8700 Leoben, Austria

[2] Rohöl-Aufsuchungs AG, Schwarzenbergplatz 16, 1015 Vienna, Austria

Introduction

Significant progress has been achieved in the last decades in the understanding of the formation, mixing and alteration of natural gas as well as of gas-oil and gas-source rock correlations. Based on the molecular and isotope composition of gas, it has been recognized that in addition to thermogenic processes and biodegradation of organic matter in pelitic rocks (primary microbial gas), commercial gas accumulation may result from biodegradation of preexisting oil and gas (secondary microbial gas) (e.g., Head et al. 2003; Jones et al. 2008; Milkov 2010, 2011).

Important parameters for the interpretation of gas data are stable carbon and hydrogen isotope ratios. Stable carbon isotopic ratios are mainly controlled by the formation mechanism (thermogenic vs. microbial), as well as the isotopic signature and thermal maturity of the source rocks (Berner and Faber 1987; Chung et al. 1988; Clayton 1991; Fuex 1977; Galimov 2006; James 1983, 1990; Krooss et al. 1995; Littke et al. 1995; Rice and Claypool 1981; Rooney et al. 1995; Schoell 1980, 1983; Stahl 1977; Whiticar 1994). Hydrogen isotope ratios are controlled by the exchange of hydrogen between water and thermally maturing organic matter (Lewan 1993, 1997; Schimmelmann et al. 2001, 2004; Yoneyama et al. 2002). In contrast, the exchange between water and already formed *n*-alkanes

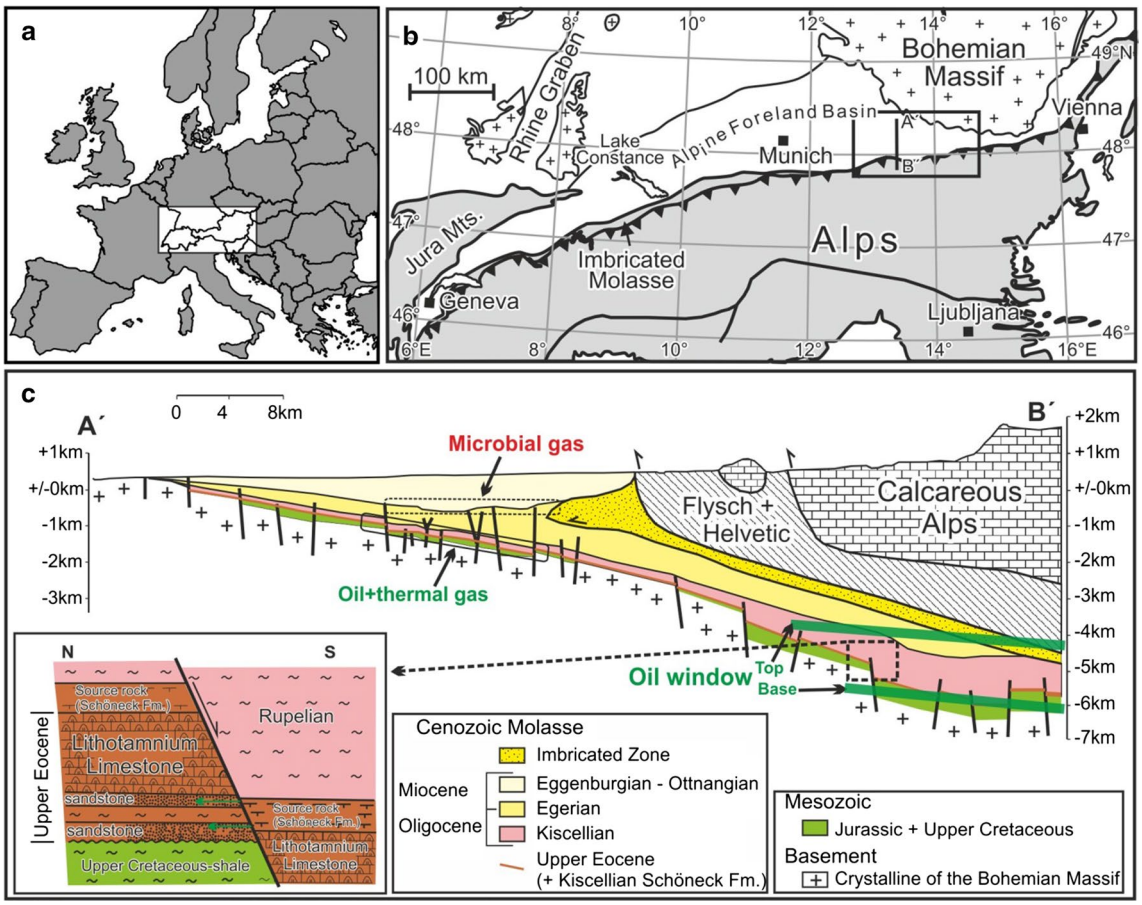

Fig. 1 **a**, **b** Location maps of study area, **c** cross section through the Alpine Foreland Basin (modified after Wagner 1996). *Inset* in **c** explains migration from source rocks into stratigraphically deeper carrier beds across normal faults (Malzer et al. 1993). See **b** for location of section

is limited (Hoering 1984; Sessions et al. 2004; Seewald et al. 1998). Enrichment in deuterium with increasing thermal stress is observed in natural samples (Dai 1990; Radke et al. 2005; Schoell 1980) as well as in theoretical and laboratory studies (e.g., Ni et al. 2011; Tang et al. 2005).

Since the pioneering work on carbon and hydrogen isotope ratios of Schoell (1977, 1984), it is known that both oil-associated thermogenic gas and microbial methane exist in the Alpine Foreland Basin, which extends along the northern margin of the Alps from Vienna to Geneva (Fig. 1a, b). According to traditional concepts, thermogenic hydrocarbons are found in Mesozoic and Eocene reservoirs, whereas microbial gas prevails in Oligocene–Miocene reservoirs separated effectively from the underlying thermogenic petroleum system by several hundred meters of shales (e.g., Brix and Schultz 1993).

However, recently Reischenbacher and Sachsenhofer (2011) emphasized that molecular and isotopic gas data from the Austrian part of the Alpine Foreland Basin are in conflict with this simple model. Actually, Pytlak et al. (2016) could show that methane associated with oil deposits in Cenomanian and Eocene reservoirs is a mixture of thermogenic, primary and secondary microbial methane. Moreover, the presence of condensate in some Oligocene–Miocene reservoirs challenges the interpretation of pure microbial gas in Oligocene–Miocene reservoirs.

The present paper focusses on gas in Upper Oligocene and Lower Miocene clastic reservoirs. Main aims of the present contribution are to determine the origin of the gas and to understand possible mixing and alteration processes. To reach this goal, gas samples from 86 wells representing all producing fields in the Austrian sector of the basin (fields labeled in Fig. 2) were studied for their molecular and isotopic composition. Note that the present paper deals with gaseous hydrocarbons and condensates will be studied in a separate paper.

Geological background

The Alpine Foreland Basin extends along the northern margin of the Alps between Geneva and Vienna (Fig. 1a,

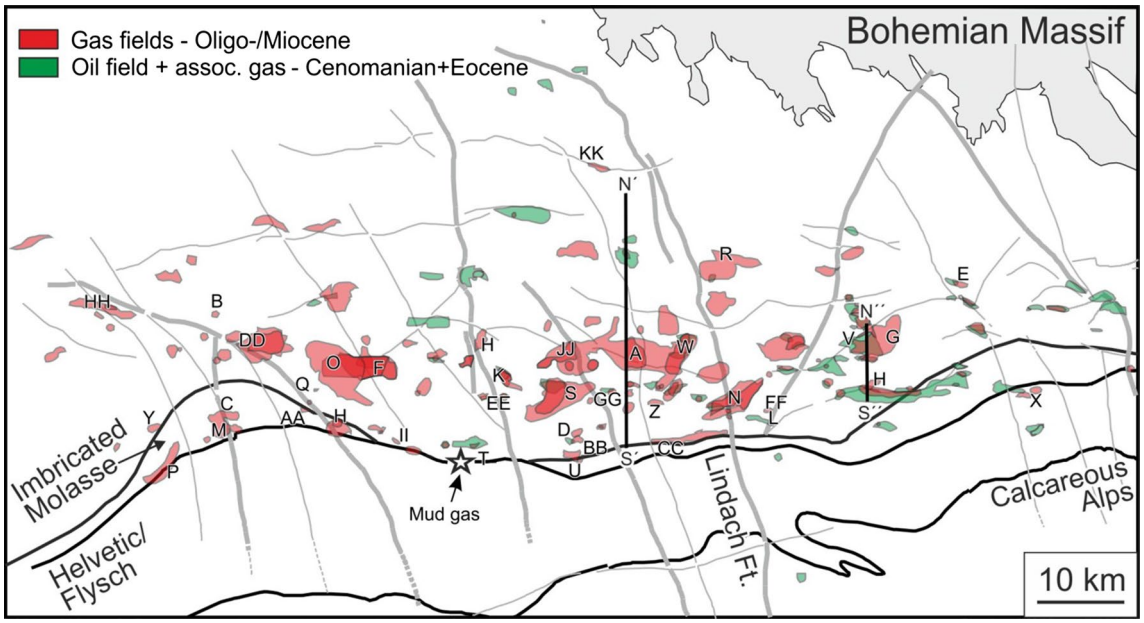

Fig. 2 Oil and gas fields in study area. *Labels* denote currently producing gas fields with Oligocene–Miocene reservoirs. Cross sections N′–S′ and N″–S″ are presented in Fig. 10a, b

b). The asymmetric basin deepens toward the south and extends below the Alpine nappes (Fig. 1c). In the Austrian sector of the Alpine Foreland Basin, the sedimentary succession overlies crystalline basement of the Bohemian Massif and comprises from bottom to top: (1) Permo-Carboniferous graben sediments, (2) Jurassic and Upper Cretaceous mixed carbonate-siliciclastic shelf sediments, and (3) Eocene to Upper Miocene Molasse sediments (Fig. 3). The Cenozoic section starts with Upper Eocene shallow-marine and fluvial carbonates, shales and sandstones. Late Eocene and Early Oligocene loading of the Alpine nappes caused down-bending of the foreland, southward increasing basement depth and rapid deepening of the depositional environment. Deep marine pelitic rocks with thin carbonate layers were deposited during Early Oligocene time (Schöneck, Dynow, Eggerding formations). Locally these rocks, about 60 m thick, have been removed by submarine erosion before deposition of the overlying Zupfing Formation. During Late Oligocene and Early Miocene times gravity flow deposits (Puchkirchen Group, lower Hall Formation; Fig. 3) accumulated in a deep marine basin-axial channel system (Puchkirchen Channel) originating in the west (near Munich) from a prograding–retrograding delta system (Covault et al. 2009; Hubbard et al. 2005, 2009). The coarse-grained clastic rocks form part of the Lower Puchkirchen Formation (uppermost Chattian to lowermost Aquitanian), the Upper Puchkirchen Formation (Aquitanian to lower Burdigalian) and the Hall Formation, which follow above a major erosional event (Grunert et al. 2013, 2015). Pelitic rocks, typically with low organic matter contents, were deposited outside of the channel system. However, organic matter-rich intervals, including a "fish shale" near the top of the Upper Puchkirchen Formation, occur as well (Wagner 1996, 1998). Decreased subsidence and increased sedimentation rates resulted in filling of the basin between late Eggenburgian and Ottnangian times. Coal-bearing freshwater sediments with a Middle to Late Miocene age dominate the top of the Cenozoic succession. Different fault systems occur in the Alpine Foreland Basin. NE–SW and NW–SE trending faults formed during Paleozoic times and were reactivated in the Mesozoic and the Paleogene. During Late Eocene and Early Oligocene times flexural down-bending resulted in the formation of W–E trending normal faults. Many of them were reactivated during the Miocene (Wagner 1996, 1998). Extensive regional uplift after Late Miocene time caused erosion of sediments, 500–900 m thick and cooling of about 20 °C (Gusterhuber et al. 2012).

Traditionally, two petroleum systems are distinguished in the Austrian part of the Alpine Foreland Basin: A thermogenic petroleum system is based on Lower Oligocene source rocks (Schöneck Fm., Eggerding Fm.; Sachsenhofer et al. 2010; Sachsenhofer and Schulz 2006; Schulz et al. 2002), which reached the oil window beneath the Alpine nappes in Miocene time (Gusterhuber et al. 2013). Main reservoirs are Cenomanian and Upper Eocene non-marine to shallow-marine sandstones in structural traps. The Lower Oligocene Schöneck Formation is also the primary seal formation (Veron 2005). The cumulative production of oil + condensate was 8903825 tons and 1647 M Nm^3

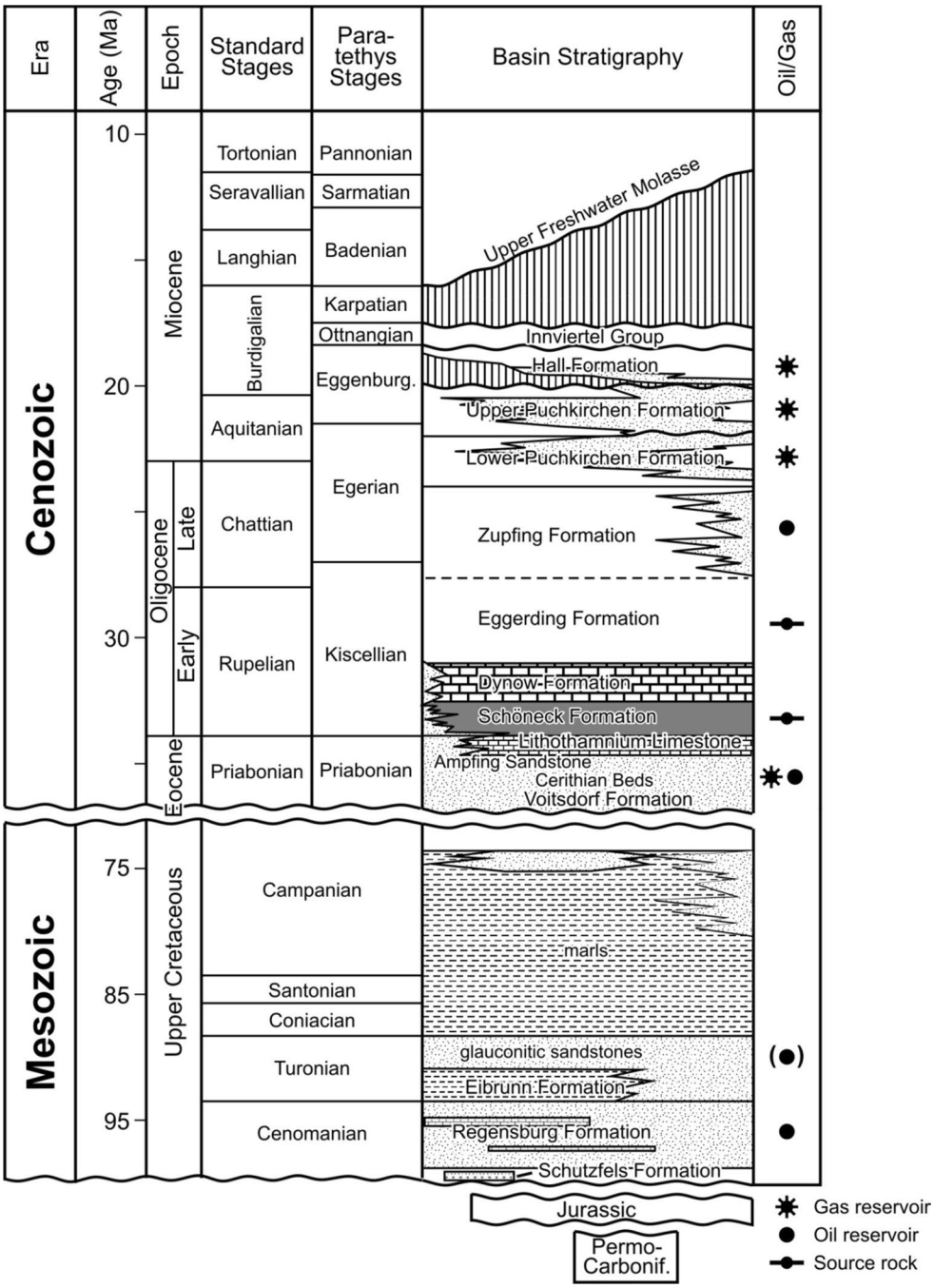

Fig. 3 Stratigraphy of Cenozoic and Mesozoic rocks in the Austrian part of the Alpine Foreland Basin (after Wagner 1996)

of associated gas (RAG production until 2015, industrial data).

Methane depleted in ^{13}C, traditionally interpreted as microbial in origin (e.g., Schoell 1984; Schulz and van Berk 2009), prevails in clastic deep water sediments with a Late Oligocene to Early Miocene age (Puchkirchen Group, Hall Fm.; Covault et al. 2009; Hubbard et al. 2005, 2009). Intraformational shales form the seals (Veron 2005). The occurrence of condensate and wet gas suggests at least local mixing with thermogenic hydrocarbons (Reischenbacher and Sachsenhofer 2011; Wagner 1998). The cumulative production from Oligocene and Miocene units was 23352 M Nm^3 of gas (RAG production until 2015, industrial data).

Sampling and analytical methods

Sampling procedure

Samples (87) have been taken from 86 wells using the IsoTube® gas sampling system. The aluminum-made sampling

cylinders were attached directly to the wellheads via the pressure reduction unit and purged with produced gas several times to avoid air contamination. Finally, the IsoTubes were filled to the maximum allowed pressure of 8 bar. In addition, mud gas data of a recently drilled well are considered in the interpretation section.

Laboratory methods

Molecular compositions of gas samples were determined by mounting the IsoTubes directly to the sampling loop of a Trace GC-ultra equipped with three various gas channels. Hydrocarbons were resolved on a 30-m Rtx-Alumina capillary column (i.d. 0.53 mm; filling Na_2SO_4, 10 µm film thickness) and detected by FID. Permanent gases were resolved on two packed columns: HayeSep Q (2 m × 1/8″ OD) and MolSieve 5A (2 m × 1/8″ OD) and detected by TCD. The column oven was programmed to hold a temperature of 50 °C for 4.3 min and then heated to 165 °C at 10 °C/min, at which point the temperature was held for 0.5 min. Helium was used as carrier gas for all three channels. Peak identification has been performed based on comparison of retention times of calibration gas mixtures and analyzed samples. Concentrations have been calculated based on peak areas against calibration gas mixtures consisting of most compounds observed in the samples.

Stable C and H isotope measurements were carried out using a Trace GC-ultra gas chromatograph attached to the ThermoFisher Delta-V isotope ratio mass spectrometer (IRMS) via a combustion and high-temperature reduction interface, respectively (GC Isolink, ThermoFisher). The GC coupled to the IRMS was equipped with a 25-m PoraPlot capillary column (i.d. 0.32 mm; 0.10 µm film thickness). The oven temperature was programmed from 30 to 180 °C at a rate of 5 °C/min followed by an isothermal period of 5 min. Helium was used as carrier gas. For calibration, a CO_2 or H_2 standard gas was injected at the beginning and at the end of each analysis. Analytical reproducibility was controlled by repeated measurements of a calibration gas. $^2H/^1H$ and $^{13}C/^{12}C$ relative ratios are expressed relative to VSMOW and VPDB, respectively.

Results

Molecular composition

The studied gas samples are dominated by methane (97.2–99.4%) with minor concentrations of C_{2+} hydrocarbons, nitrogen (0.2–2.1%) and carbon dioxide (<0.5%). In few samples traces of ethene and/or propene were detected (Table 1). Traces of different C_{5+} isomers have been detected, but only some of them have been quantified (Fig. 4). Thus, results reported in Table 1 were not normalized to 100%.

Gas dryness, defined by $C_1/(C_2 + C_3)$ (Bernard et al. 1978), varies between 96 and 471 with an average value of 228. An exceptional dry gas (~4400) is produced from the KK field (Fig. 5) in the northern part of the basin (see Fig. 2 for location).

Ratios of branched versus straight *n*-alkanes range between 0.9 and 4.4 for butanes and 1.9 and 19.8 for pentanes, respectively.

Isotopic composition

The stable carbon isotopic composition of methane varies widely from −48.5 to −65.1‰. Methane, most enriched in ^{13}C has been found in the F–O fields located in the western part of study area (Table 1; Fig. 5), whereas methane, most depleted in ^{13}C is from the KK field. δ^2H of methane ranges between −178 and −221‰ (Fig. 6). Similarly to $\delta^{13}C$ distribution, methane with elevated ^2H content occurs in the F–O fields. In addition, methane enriched in ^2H is recorded in gas from the X field (Table 1).

C_2 (−55.7 to −33‰), C_3 (−38.5 to −24.5‰) to *n*-C_4 (−33.4 to −17‰) hydrocarbons show a decreasing variability in stable carbon isotope ratios (Table 1).

Stable isotope ratios of methane obtained in the present study show a wider range of values than carbon (−59.7 to −63.3‰) and hydrogen isotope ratios (−197 to −212‰) reported by Schoell (1984) and Schulz and van Berk (2009). This is because these authors coincidently did not sample wells with isotopically heavy methane.

Interpretation and discussion

Microbial versus thermogenic gas

The driest gas is present in the KK field, where only methane and traces of ethane are observed. Moreover, methane from this field is characterized by the most negative carbon isotopic values (Fig. 5; Table 1). This suggests a pure microbial origin of the KK gas, located in the shallow northern flank of the basin, and confirms the established models (e.g., Brix and Schultz 1993; Schoell 1984). Interestingly, ethane from KK gas is isotopically lighter than that of oil-associated gas from Mesozoic and Eocene reservoirs (Fig. 7, Pytlak et al. 2016).

All other gas samples contain hydrocarbons up to *n*-hexane and yield significantly lower dryness values. Moreover, a significant number of them display isotope values characteristic for varying contributions of thermogenic hydrocarbons (Figs. 5, 6). Carbon isotope values as low as −48.5‰ (Fig. 5) indicate the presence of the highest amount of

Table 1 Molecular and isotopic composition of sampled gas

Well	TVDSS	Formation	CH_4	C_2H_6	C_3H_8	*i*-C_4H_{10}	*n*-C_4H_{10}	*i*-C_5H_{12}	*n*-C_5H_{12}	*n*-C_6H_{14}+	CO_2	N_2	$\delta^{13}C_{CH_4}$	$\delta^{13}C_{C_2H_6}$	$\delta^{13}C_{C_3H_8}$	$\delta^{13}C_{n\text{-}C_4H_{10}}$	$\delta^{13}C_{i\text{-}C_4H_{10}}$	$\delta^{13}C_{CO_2}$	$\delta^{2}H_{CH_4}$
A-1	1171	Upper P.F.	98.55	0.404	0.124	0.046	0.019	0.025	0.006	0.002	0.213	0.489	−59.0	−47.2	−33.8	−25.2	−26.0	−6.0	−205
A-2	606	H.F.	98.34	0.338	0.114	0.045	0.014	0.019	0.004	0.000	0.008	0.482	−62.5	−41.9	−29.3	−22.7	−23.2	−8.2	−198
A-3	1182	Upper P.F.	97.99	0.416	0.123	0.043	0.020	0.026	0.006	0.002	0.073	0.497	−58.0	−48.8	−35.0	−26.0	−26.5	−5.9	−207
A-4	1165	Upper P.F.	98.20	0.482	0.202	0.081	0.029	0.041	0.009	0.002	0.131	0.602	−59.5	−45.7	−34.5	−27.5	−27.9	−5.7	−205
A-5	1169	Upper P.F.	98.37	0.424	0.147	0.049	0.021	0.027	0.007	0.002	0.160	0.507	−59.0	−47.0	−35.0	−26.3	−26.4	−5.7	−206
A-6	1167	Upper P.F.	98.57	0.405	0.131	0.045	0.024	0.027	0.007	0.003	0.106	0.511	−59.8	−45.9	−35.3	−25.8	−24.5	−6.7	−205
A-7	1399	Upper P.F.	97.86	0.545	0.220	0.103	0.031	0.041	0.008	0.002	0.103	0.674	−57.8	−45.8	−34.6	−31.1	−30.3	−5.7	−202
B-1	802	H.F.	98.29	0.349	0.162	0.046	0.018	0.020	0.005	0.001	0.020	0.617	−58.4	−48.6	−33.0	−21.9	−22.0	18.0	−210
C-1	749	Upper P.F.	98.40	0.206	0.052	0.017	0.005	0.007	0.002	0.001	0.009	0.393	−62.0	−55.7	−36.0	−25.0	−24.2	−6.5	−221
D-1	1021	Upper P.F.	98.19	0.358	0.106	0.032	0.018	0.021	0.005	0.001	0.041	0.430	−57.6	−49.2	−24.7	−26.2	−22.0	5.0	−204
E-1	33	H.F.	98.92	0.277	0.081	0.022	0.007	0.006	0.001	0.000	0.035	0.653	−62.7	−38.0	−26.8	−24.0	−22.0	−38.0	−204
F-1	1093	Upper P.F.	98.61	0.332	0.160	0.058	0.048	0.033	0.016	0.004	0.076	0.777	−61.4	−42.8	−31.0	−26.0	−24.7	−4.0	−201
F-2	690	H.F.	98.80	0.327	0.124	0.044	0.018	0.020	0.005	0.001	0.072	0.560	−60.5	−46.3	−31.9	−26.0	−24.2	3.0	−202
F-3	1694	Upper P.F.	97.68	0.687	0.335	0.126	0.064	0.072	0.016	0.004	0.298	0.766	−59.6	−43.5	−35.5	−30.9	−30.2	−1.3	−203
F-4	1061	Upper P.F.	98.28	0.356	0.106	0.033	0.022	0.018	0.006	0.002	0.069	0.516	−48.5	−38.0	−29.4	−27.2	−25.4	0.1	−185
F-5	702	H.F.	98.40	0.363	0.108	0.033	0.020	0.023	0.007	0.002	0.098	0.459	−56.1	−43.2	−33.5	−28.8	−23.5	−1.4	−180
F-6	691	H.F.	98.54	0.327	0.126	0.044	0.019	0.019	0.005	0.001	0.007	0.616	−50.3	−41.1	−31.6	−29.4	−26.3	−0.3	−193
G-1	234	H.F.	98.94	0.304	0.100	0.029	0.012	0.013	0.003	0.000	0.062	0.516	−63.5	−38.5	−25.7	−25.8	−24.7	−7.1	−202
H-1	305	H.F.	98.65	0.253	0.074	0.018	0.006	0.007	0.002	0.001	0.057	0.471	−61.6	-36.4	−24.5	−17.0	−17.8	−3.8	−199
I-1	627	H.F.	98.73	0.330	0.113	0.035	0.014	0.015	0.004	0.001	0.063	0.420	−60.0	−49.6	−32.0	−26.0	−25.2	4.5	−201
I-2	695	Upper P.F.	98.82	0.272	0.082	0.019	0.010	0.009	0.003	0.001	0.030	0.373	−59.3	−50.8	−34.1	−26.0	−25.0		−212
I-3	689	Upper P.F.	98.42	0.263	0.075	0.019	0.010	0.010	0.003	0.002	0.036	0.376	−58.9	−51.3	−33.2	−25.5	−22.0	4.0	−211
J-1	1410	Upper P.F.	97.24	0.484	0.221	0.071	0.027	0.043	0.009	0.004	0.261	0.725	−61.6	−38.8	−35.7	−25.2	−23.6	−7.4	−204
K-1	1151	Upper P.F.	98.29	0.371	0.113	0.033	0.017	0.022	0.006	0.002	0.407	0.422	−57.4	−50.8	−33.7	−28.0	−27.7	−7.0	−205
L-1	398	H.F.	99.41	0.273	0.125	0.029	0.011	0.012	0.003	0.005	0.046	0.464	−60.2	−45.1	−30.5	−25.3	−23.5	−7.9	−206
M-1	714	Upper P.F.	98.46	0.169	0.067	0.016	0.007	0.006	0.001	0.000	0.029	0.447	−60.7	−51.6	−34.2	−31.9	−30.8	−10.0	−212
M-2	629	Upper P.F.	98.71	0.311	0.065	0.013	0.005	0.005	0.002	0.000	0.114	0.493	−60.9	−54.1	−33.6	−26.0	−23.4	−16.0	−216
M-3	742	Upper P.F.	98.77	0.267	0.052	0.013	0.005	0.006	0.002	0.001	0.064	0.480	−61.0	−53.4	−35.6	−26.0	−24.6	−17.0	−218
M-4	763	Upper P.F.	98.92	0.254	0.070	0.016	0.007	0.007	0.002	0.000	0.038	0.407	−62.1	−52.2	−34.7	−33.4	−29.9	−9.1	−202
M-5	571	Upper P.F.	98.39	0.226	0.054	0.014	0.008	0.006	0.002	0.000	0.085	0.391	−60.3	−52.2	−33.9	−30.9	−29.3	−10.8	−205
M-6	577	Upper P.F.	97.75	0.262	0.049	0.012	0.005	0.006	0.002	0.001	0.119	0.468	−60.4	−46.0	−34.0	−26.0	−22.4	−15.5	−221
N-1	446	H.F.	98.33	0.318	0.102	0.036	0.010	0.013	0.001	0.003	0.166	0.401	−60.0	−47.5	−28.7	−27.0	−24.0	−8.6	−203
N-2	335	H.F.	99.05	0.317	0.097	0.019	0.006	0.008	0.000	0.000	0.026	0.480	−60.5	−47.2	−31.0	−25.5	−22.0	−8.9	−202
N-3	360	H.F.	98.83	0.302	0.090	0.019	0.006	0.018	0.001	0.000	0.038	0.693	−60.9	−49.6	−30.4	−25.5	−25.0	−4.0	−200
O-1	690	H.F.	97.97	0.319	0.127	0.032	0.011	0.014	0.003	0.000	0.154	0.471	−59.7	−49.9	−33.6	−31.0	−29.9	−9.2	−189

Table 1 continued

Well	TVDSS	Formation	CH_4	C_2H_6	C_3H_8	*i*-C_4H_{10}	*n*-C_4H_{10}	*i*-C_5H_{12}	*n*-C_5H_{12}	*n*-C_6H_{14}+	CO_2	N_2	$\delta^{13}C_{CH_4}$	$\delta^{13}C_{C_2H_6}$	$\delta^{13}C_{C_3H_8}$	$\delta^{13}C_{n\text{-}C_4H_{10}}$	$\delta^{13}C_{i\text{-}C_4H_{10}}$	$\delta^{13}C_{CO_2}$	$\delta^{2}H_{CH_4}$
O-2	673	H.F.	98.00	0.319	0.099	0.036	0.015	0.015	0.003	0.001	0.102	0.566	−55.3	−39.4	−30.6	−27.8	−26.7	−6.4	−187
O-3	744	H.F.	97.84	0.326	0.101	0.032	0.013	0.014	0.003	0.001	0.034	0.485	−49.6	−40.8	−31.8	−29.5	−26.0	−6.9	−200
O-4	776	H.F.	98.47	0.427	0.144	0.054	0.022	0.027	0.006	0.002	0.127	0.506	−54.3	−43.3	−32.1	−28.3	−27.2	−8.2	−189
O-5	700	H.F.	98.76	0.326	0.116	0.034	0.011	0.013	0.002	0.000	0.024	0.480	−52.5	−43.4	−33.9	−28.9	−26.4	−10.8	−205
O-6	698	H.F.	97.89	0.328	0.123	0.034	0.014	0.015	0.004	0.001	0.054	0.488	−53.7	−42.1	−29.9	−27.8	−25.7	−8.2	−192
O-7	679	H.F.	97.56	0.317	0.120	0.030	0.009	0.011	0.002	0.000	0.082	0.580	−55.0	−44.9	−31.3	−28.7	−27.3	−8.0	−197
P-1	797	Upper P.F.	98.47	0.281	0.040	0.011	0.004	0.005	0.002	0.002	0.072	0.241	−54.5	−42.9	−31.2	−29.3	−28.5	1.8	−187
P-2	1045	Upper P.F.	98.77	0.282	0.042	0.005	0.003	0.002	0.001	0.000	0.052	0.219	−64.4	−55.1	−31.6		−27.9	−7.1	−178
Q-1	1610	Upper P.F.	98.45	0.408	0.140	0.046	0.018	0.018	0.003	0.000	0.004	0.578	−60.3	−47.9	−34.7	−27.8	−28.0		−207
R-1	273	H.F.	97.96	0.326	0.083	0.023	0.013	0.011	0.005	0.004	0.035	0.558	−61.3	−42.7	−28.8	−23.2	−22.0	−6.5	−202
R-2	254	H.F.	97.99	0.325	0.077	0.021	0.010	0.008	0.002	0.000	0.021	0.561	−61.6	−42.9	−28.5	−21.8	−20.2	−7.7	−202
R-3	317	H.F.	97.56	0.329	0.080	0.025	0.011	0.011	0.002	0.000	0.000	0.504	−61.3	−43.0	−28.4	−20.6	−22.3		−202
R-4	275	H.F.	98.74	0.322	0.088	0.025	0.011	0.012	0.003	0.000	0.016	0.613	−62.6	−43.5	−29.5	−23.1	−23.5	−7.0	−202
R-5	284	H.F.	97.33	0.293	0.080	0.022	0.010	0.010	0.002	0.000	0.024	0.596	−63.0	−43.2	−28.4	−18.3	−21.1	−3.0	−201
S-1	447	H.F.	98.95	0.295	0.121	0.028	0.010	0.010	0.002	0.000	0.018	0.557	−60.7	−44.5	−28.8	−21.0	−21.0	−5.0	−203
S-2	1184	Upper P.F.	98.40	0.371	0.146	0.043	0.023	0.024	0.008	0.003	0.252	0.446	−58.1	−48.1	−34.6	−27.5	−27.5	−3.4	−207
S-3	1180	Upper P.F.	97.70	0.363	0.142	0.040	0.019	0.026	0.006	0.000	0.075	0.438	−57.8	−48.9	−34.2	−23.8	−24.4	4.2	−206
S-4	604	H.F.	98.99	0.333	0.110	0.028	0.018	0.018	0.006	0.002	0.038	0.439	−58.2	−51.0	−34.0	−28.0	−25.0	−11.0	−205
T-1	795	Upper P.F.	98.05	0.324	0.109	0.028	0.013	0.016	0.004	0.001	0.045	0.455	−63.8	−49.0	−27.3	−25.3	−22.8	0.0	−190
U-1	814	Upper P.F.	98.19	0.339	0.165	0.036	0.025	0.021	0.007	0.001	0.021	0.412	−59.3	−49.2	−34.0	−26.8	−26.4	−6.5	−204
U-2	739	Upper P.F.	98.48	0.334	0.161	0.036	0.026	0.022	0.008	0.002	0.064	0.399	−60.0	−46.5	−31.3	−25.0	−23.4	−7.3	−203
U-3	1037	Upper P.F.	98.44	0.363	0.222	0.044	0.034	0.030	0.009	0.002	0.044	0.725	−61.8	−49.7	−33.9	−25.7	−26.0	−6.0	−197
V-1	375	H.F.	98.88	0.260	0.087	0.024	0.007	0.010	0.002	0.000	0.054	0.498	−60.2	−33.0	−26.0	−25.8	−25.7	−6.0	−209
V-2	228	H.F.	98.82	0.323	0.148	0.037	0.029	0.019	0.010	0.008	0.055	0.547	−62.1	−36.0	−27.3	−27.2	−27.4	−8.0	−201
W-1	489	H.F.	97.46	0.503	0.195	0.086	0.026	0.038	0.007	0.002	0.068	0.633	−57.9	−45.8	−34.2	−25.8	−28.9	−9.0	−202
W-2	498	H.F.	97.85	0.472	0.151	0.071	0.029	0.040	0.010	0.003	0.394	0.511	−56.0	−46.0	−34.8	−28.9	−29.2	−2.6	−208
W-3	1156	Upper P.F.	97.61	0.537	0.209	0.096	0.029	0.037	0.007	0.002	0.131	0.656	−57.6	−45.4	−34.6	−28.4	−28.7	−7.8	−202
W-4	1162	Upper P.F.	97.99	0.448	0.128	0.051	0.021	0.025	0.006	0.002	0.235	0.490	−56.9	−46.3	−34.7	−28.2	−28.6	−6.0	−210
X-1	30	Imbr.Mol.	98.46	0.534	0.010	0.017	0.004	0.001	0.001	0.000	0.037	0.631	−62.8	−38.0	−25.2	−25.5	−20.4	−3.4	−187
X-2	190	Imbr.Mol.	98.01	0.678	0.135	0.036	0.015	0.014	0.003	0.000	0.022	0.567	−60.3	−43.3	−33.0	−26.9	−27.3	−3.0	−184
X-3	193	Imbr.Mol.	98.36	0.458	0.097	0.014	0.005	0.004	0.001	0.000	0.018	0.629	−61.5	−48.9	−36.0	−26.5	−25.5	−4.1	−180
X-4	−21	Imbr.Mol.	98.41	0.182	0.026	0.004	0.001	0.000	0.000	0.000	0.019	0.666	−63.2	−55.5	−38.5	−26.0	−21.5	−1.2	−182
Y-1	2026	Lower P.F.	98.07	0.432	0.215	0.078	0.024	0.028	0.008	0.002	0.152	0.427	−63.3	−51.8	−37.3	−33.1	−31.7	−10.9	−187
Z-1	544	H.F.	98.11	0.301	0.113	0.031	0.014	0.014	0.003	0.001	0.032	0.428	−59.7	−46.0	−30.0	−24.0	−27.0	−2.0	−204
AA-1	628	H.F.	98.17	0.281	0.103	0.033	0.011	0.013	0.002	0.001	0.074	0.523	−59.8	−47.7	−31.0	−23.0	−22.0	−0.4	−209
BB-1	463	H.F.	98.66	0.294	0.129	0.031	0.013	0.015	0.003	0.000	0.004	0.480	−60.8	−44.3	−29.7	−19.2	−20.8	−6.2	−201

Table 1 continued

Well	TVDSS	Formation	CH_4	C_2H_6	C_3H_8	*i*-C_4H_{10}	*n*-C_4H_{10}	*i*-C_5H_{12}	*n*-C_5H_{12}	*n*-C_6H_{14}+	CO_2	N_2	$\delta^{13}C_{CH_4}$	$\delta^{13}C_{C_2H_6}$	$\delta^{13}C_{C_3H_8}$	$\delta^{13}C_{n\text{-}C_4H_{10}}$	$\delta^{13}C_{i\text{-}C_4H_{10}}$	$\delta^{13}C_{CO_2}$	$\delta^{2}H_{CH_4}$
CC-1	335	H.F.	99.45	0.314	0.124	0.037	0.014	0.012	0.002	0.002	0.010	0.522	−60.3	−48.8	−31.0	−23.0	−23.0	−11.1	−201
DD-1	1454	Lower P.F.	97.95	0.416	0.133	0.041	0.018	0.024	0.006	0.001	0.217	0.393	−57.0	−46.8	−32.4	−30.6	−29.8	−6.7	−186
DD-1	1278	Upper P.F.	98.50	0.341	0.065	0.014	0.017	0.022	0.006	0.001	0.013	0.457	−59.0	−50.2	−35.1	−31.6	−30.0	−13.1	−189
EE-1	594	H.F.	98.47	0.291	0.101	0.039	0.012	0.014	0.003	0.000	0.079	0.448	−60.2	−43.6	−29.0	−21.0	−22.0	−2.0	−200
FF-1	1185	Upper P.F.	98.50	0.441	0.109	0.040	0.016	0.032	0.006	0.024	0.039	0.597	−54.6	−49.1	−32.4	−27.0	−28.0	−13.0	−199
GG-1	493	H.F.	99.11	0.262	0.102	0.032	0.010	0.011	0.001	0.001	0.087	0.367	−60.3	−48.4	−30.9		−24.8	−9.8	−198
GG-2	505	H.F.	98.76	0.325	0.131	0.032	0.014	0.013	0.003	0.003	0.052	0.655	−60.1	−43.8	−29.8	−24.0	−23.0	−9.3	−200
HH-1	1261	Upper P.F.	98.09	0.326	0.109	0.035	0.016	0.020	0.005	0.001	0.117	0.513	−58.4	−46.1	−32.1	−26.0	−26.7	1.2	−205
II-1	419	H.F.	98.53	0.321	0.026	0.006	0.001	0.002	0.000	0.000	0.000	0.536	−62.0	−49.6	−27.0				−195
II-2	623	H.F.	97.99	0.302	0.028	0.006	0.002	0.002	0.000	0.000	0.000	0.539	−60.7	−50.0	−27.3				−195
JJ-1	1201	Upper P.F.	97.81	0.390	0.118	0.035	0.019	0.024	0.006	0.002	0.239	0.463	−57.6	−49.7	−35.4	−26.0	−26.0	−4.1	−206
JJ-2	1181	Upper P.F.	97.71	0.387	0.121	0.036	0.019	0.024	0.006	0.003	0.335	0.448	−57.7	−48.9	−35.1	−26.0	−26.4	−5.5	−207
JJ-3	1180	Upper P.F.	97.58	0.391	0.115	0.034	0.019	0.025	0.006	0.000	0.456	0.463	−57.7	−49.7	−35.0	−24.5	−24.0	−6.2	−207
JJ-4	1186	Upper P.F.	97.21	0.390	0.110	0.036	0.019	0.025	0.007	0.002	0.271	0.461	−57.7	−49.1	−35.3	−26.9	−27.2	−4.6	−208
KK-1	102	Upper P.F.	97.47	0.023	0.000	0.000	0.000	0.000	0.000	0.000	0.002	1.806	−65.1	−47.9					−214
KK-2	116	Upper P.F.	97.93	0.022	0.000	0.000	0.000	0.000	0.000	0.000	0.002	2.106	−64.5	−42.3					−211

Due to confidentiality, in column "Well" true names are substituted by letters corresponding to fields (see Fig. 10) and digits to certain wells

TVDSS true vertical depth subsea, *H.F.* Hall Formation, *Upper P.F.* Upper Puchkirchen Formation, *Lower P.F.* Lower Puchkirchen Formation, *Imbr.Mol.* Imbricated Molasse

thermogenic methane in the F–O fields. Apart from wet gas, some wells produce even liquid hydrocarbons (condensates), another proof for the presence of thermogenic input (Pytlak et al. 2014; Wagner 1998). Traces of higher hydrocarbons are also visible in total gas composition (Fig. 4). Interestingly, gas dryness in Puchkirchen and Hall reservoirs with liquid hydrocarbons is often relative high (>200; Fig. 5).

Ethane in many samples is strongly depleted in ^{13}C (Fig. 7). This suggests that most of the detected ethane is microbial in origin. Actually, ethane and propane can be generated by microbial activity, although their contribution

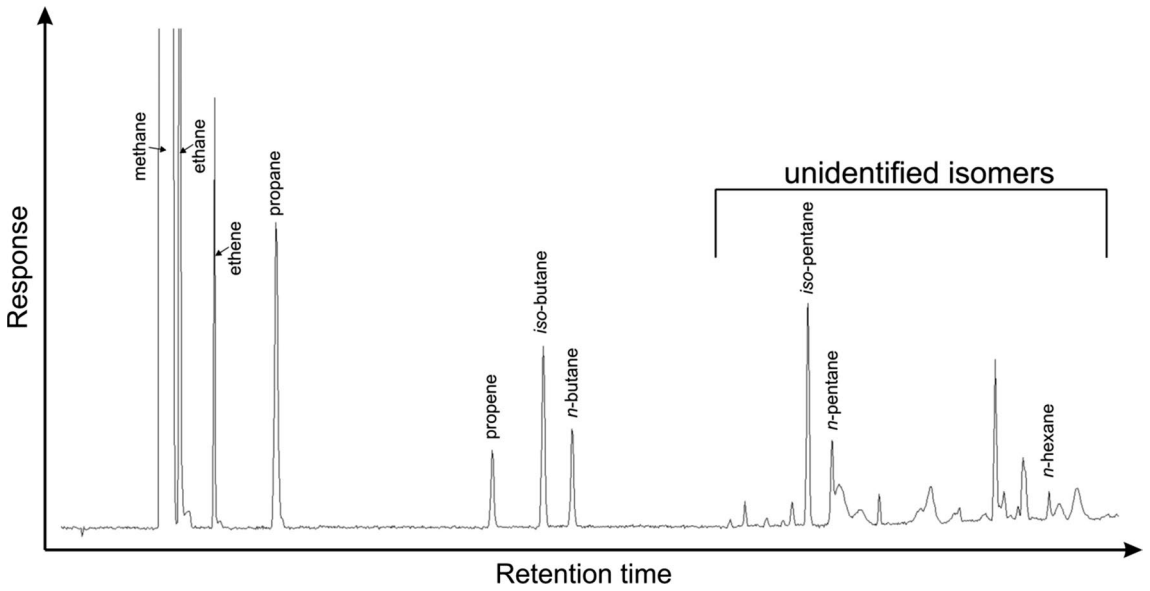

Fig. 4 Flame ionization detector (FID) chromatogram of gas sample from gas field F. For location see Fig. 2

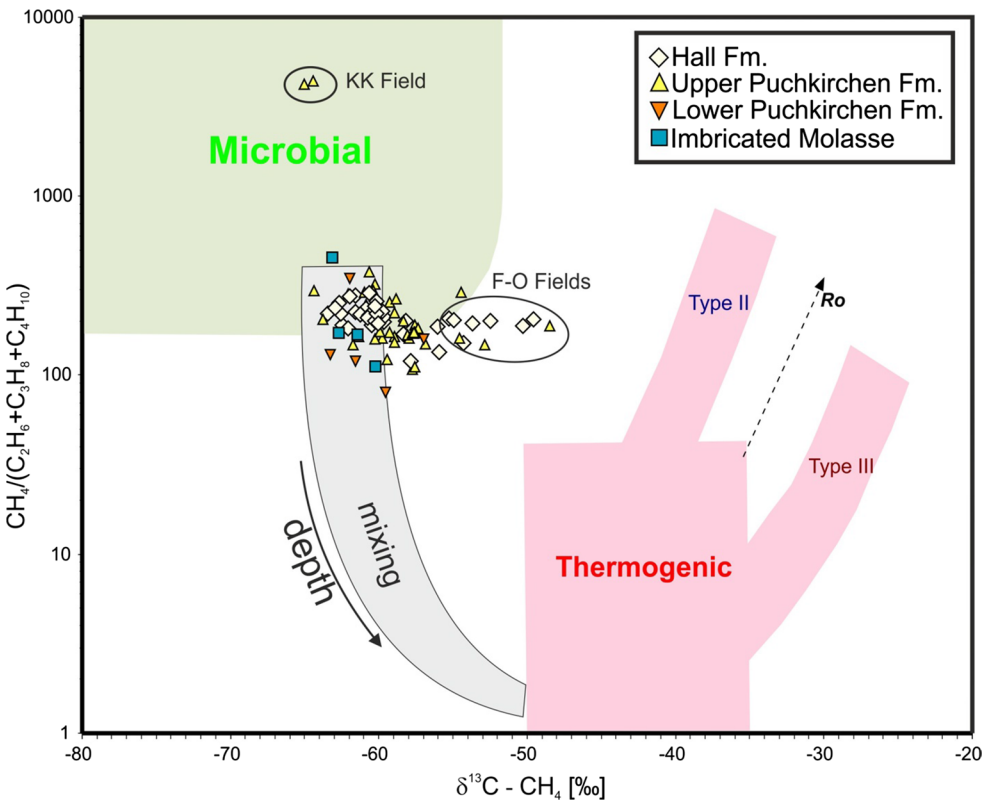

Fig. 5 Genetic characterization of oil-associated gas from the Austrian part of the Alpine Foreland Basin (discrimination diagram adopted form Bernard et al. 1978; Whiticar and Suess 1990). Note that *y* axis of original plot is expressed as $CH_4/(C_2H_6 + C_3H_8)$. Mixing trend with depth is determined by results of mud gas measurements from well-penetrating Imbricated Molasse (unpublished industrial data, for location see Fig. 2)

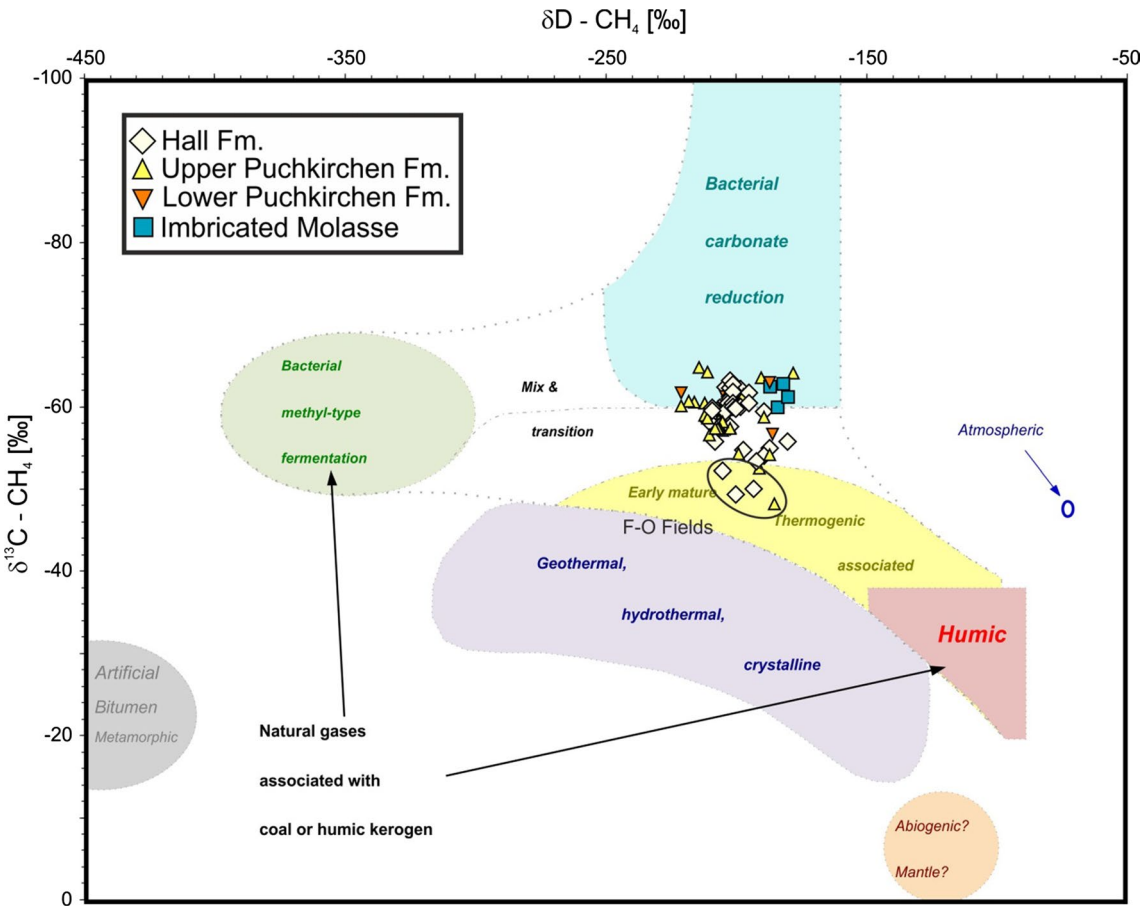

Fig. 6 Genetic characterization of gas from Oligocene–Miocene reservoirs in the Austrian part of the Alpine Foreland Basin (plot modified after Whiticar et al. 1986)

in total gas composition is typically very low (Hinrichs et al. 2006; Oremland et al. 1988; Rice and Claypool 1981).

Origin of thermogenic hydrocarbons

Figure 8a shows that gas dryness decreases with reservoir depth implying a downward increase in thermogenic hydrocarbons (see also Reischenbacher and Sachsenhofer 2011). Potentially these hydrocarbons may have been generated locally in pelitic rocks within the studied succession (or below) or may have been derived from oil-bearing deeper horizons (e.g., Eocene reservoir rocks).

The Cenozoic succession includes potential source rocks. However, these are immature north of the Alpine front (e.g., Gusterhuber et al. 2012, 2013). This is not only valid for Lower Oligocene source rocks, but also for "fish shales" near the top of the Upper Puchkirchen Formation containing up to 3.5% TOC (Belaed 2007).

Therefore, it is likely that the thermogenic hydrocarbons migrated upward from Eocene carrier beds and reservoir rocks (e.g., Wagner 1998). Although commercial oil deposits in the western part of the study area are missing, industry data show that wet gas and oil stains within Eocene horizons have been detected in the entire study area.

The plot of $\delta^{13}C$ of ethane versus $\delta^{13}C$ of propane (Berner and Faber 1996; Fig. 9) is often used to determine the maturity of gases. The data from Oligocene–Miocene reservoirs are generally shifted toward light $\delta^{13}C$ values of ethane (Fig. 9). This may indicate a contribution of microbial ethane. Moreover, propane may be enriched in ^{13}C due to biodegradation (see "Gas biodegradation and secondary microbial methane" section). Nevertheless, propane and *n*-butane isotope ratios are similar to those measured in oil-associated gas from Mesozoic and Eocene reservoirs (Pytlak et al. 2016; Fig. 7), suggesting oil-window maturity.

Controls of mixing of thermogenic and microbial gas

Whereas the microbial component of the gas has been generated locally within the Upper Oligocene to Lower Miocene succession (Schulz and van Berk 2009), the

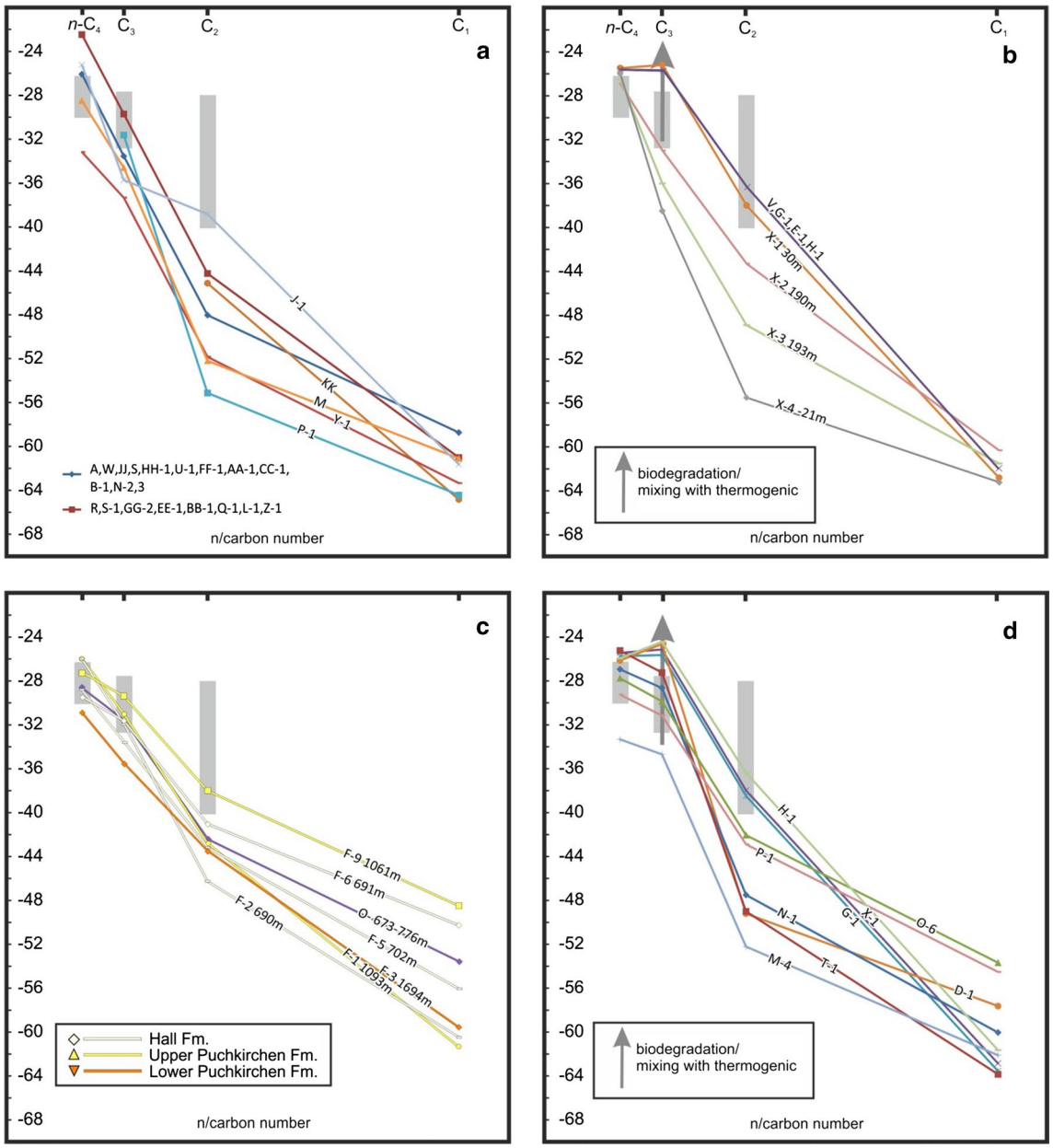

Fig. 7 Natural gas plots (Chung et al. 1988) showing the carbon isotopic compositions of individual hydrocarbons as a function of the carbon number. Depths are true vertical depth subsea (TVDSS) expressed in meters. *Gray bars* indicate isotopic signature of hydrocarbons associated with oil deposits in the Austrian part of Alpine Foreland Basin (Pytlak et al. 2016)

thermogenic fraction migrated vertically upward from Mesozoic and Eocene carrier beds and/or reservoirs. Migration may have occurred (1) along relative permeable faults or (2) within low-permeability rocks along subseismic fractures.

1. Samples G-1, E-1, H-1 and gas from a V field produce methane from Hall reservoirs in the eastern part of the study area. $\delta^{13}C$ values of methane in these fields are characteristic for microbial origin, while those of C_2 to C_4 hydrocarbons are characteristic for thermogenic, oil-associated gas (Fig. 7b). The producing Hall horizons in the above fields are located above or close to oil deposits in Eocene strata. Faults were active in the Alpine Foreland Basin during different times. In some areas fault activity stopped already during deposition of the Lower Puchkirchen Formation, whereas in others it continued till Eggenburgian time (Fig. 10). These

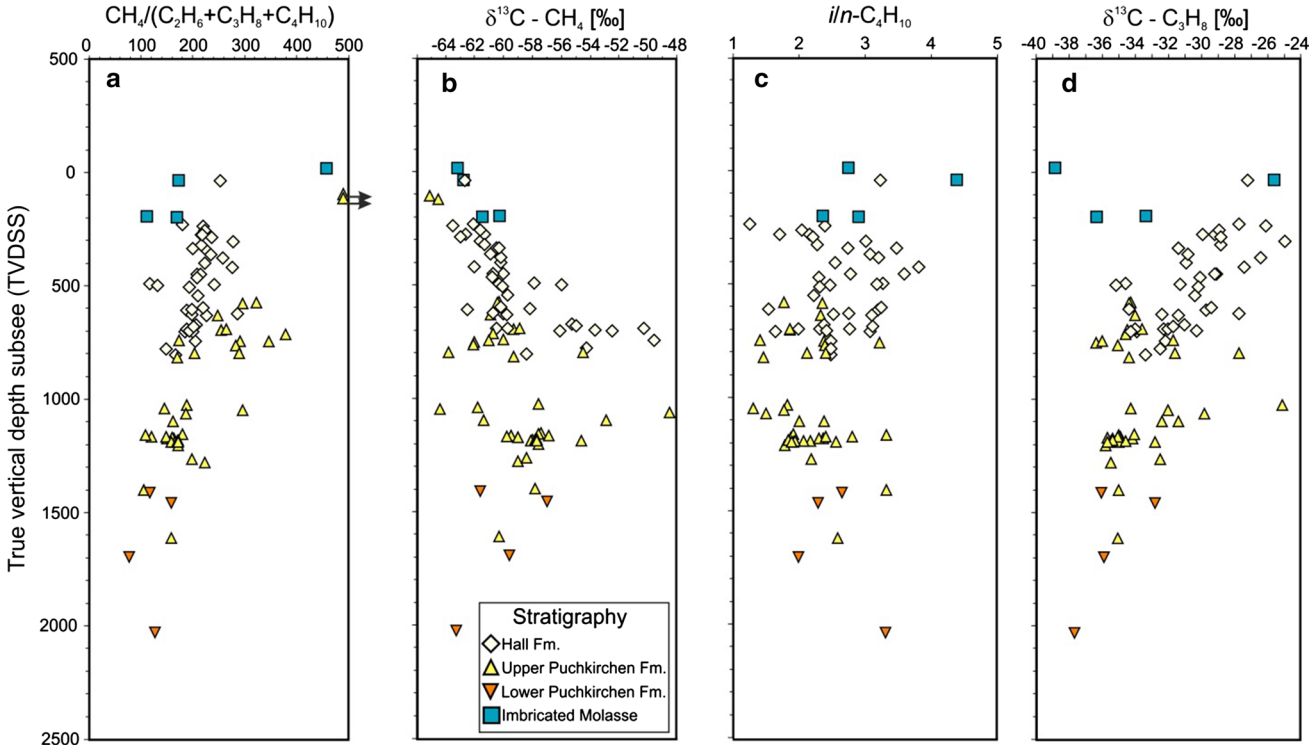

Fig. 8 Depth distribution of selected geochemical parameters. i/n-C_4H_{10} ratios >1 indicate that all gases are biodegraded. However, dryness and $\delta^{13}C$–C_3H_8 trends indicate that biodegradation decreases with depth

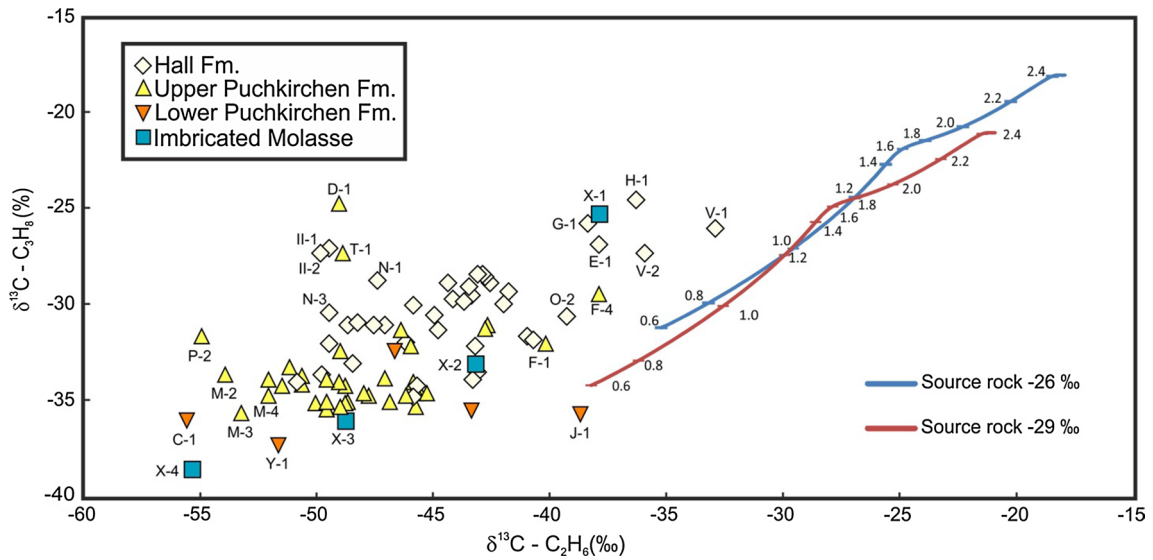

Fig. 9 Relative gas maturity base $\delta^{13}C$ distribution in ethane and propane (plot modified after Berner and Faber 1996)

long-lived faults provided potential migration pathways connecting Eocene reservoirs and the Hall Formation (Wagner 1998).

2. In areas without distinct faults, migration may have occurred through low-permeability caprocks along subseismic fractures, silty intervals and/or by diffusion. It is likely that upward migration may be facilitated in areas where lower Oligocene fine-grained rocks are eroded and along the Puchkirchen Channel system, where a high percentage of permeable clastic rocks have been deposited. Within this context, it is remarkable to observe that the F–O fields containing

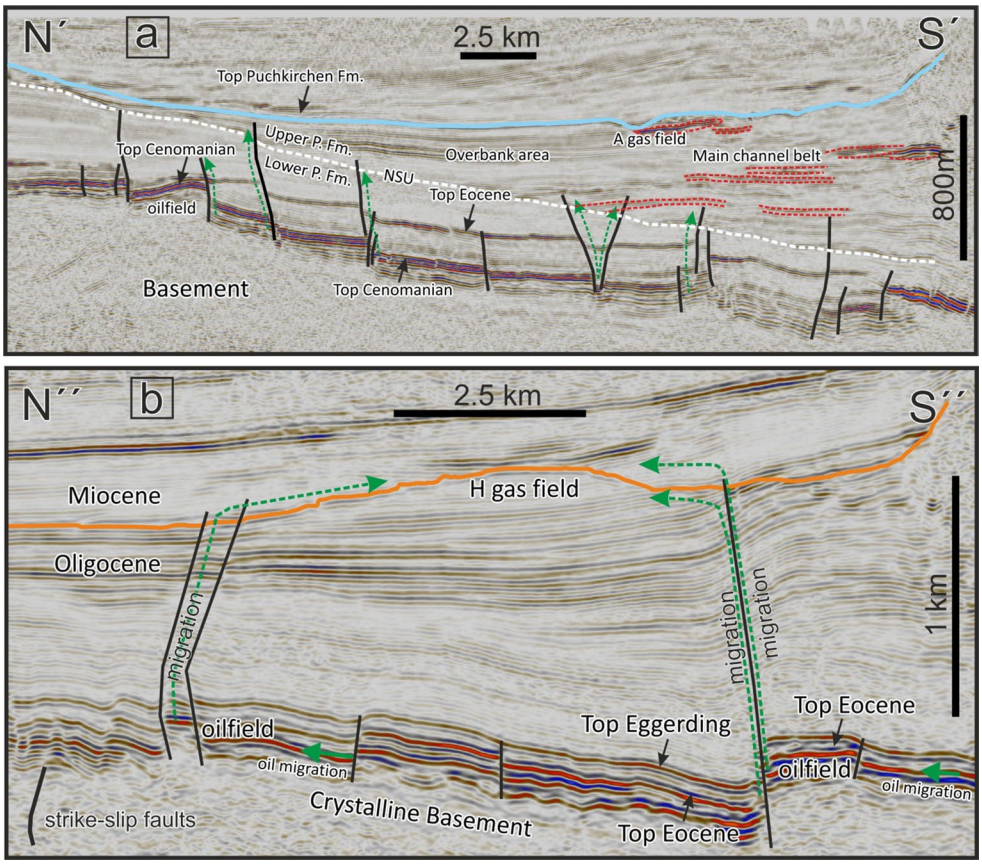

Fig. 10 Seismic examples of the Alpine Foreland Basin (for location see Fig. 2). **a** Across gas field A. Location of Puchkirchen Channel belt and adjacent overbank deposits (both are the main gas reservoirs) are indicated with *dashed red lines*. Northern Slope Unconformity (NSU, Masalimova et al. 2015) separates Lower Puchkirchen Formation (Lower P. Fm.) from Upper Puchkirchen Formation (Upper P. Fm.). The NSU is cross-cut by faults active during deposition of Upper Puchkirchen Formation providing potential migration pathways for thermogenic hydrocarbons (*dashed green lines*). **b** Across gas field H and oil fields. Majority of oil and thermogenic gas in the Alpine Foreland Basin are trapped in Cenomanian and Eocene reservoirs in fault-related structures

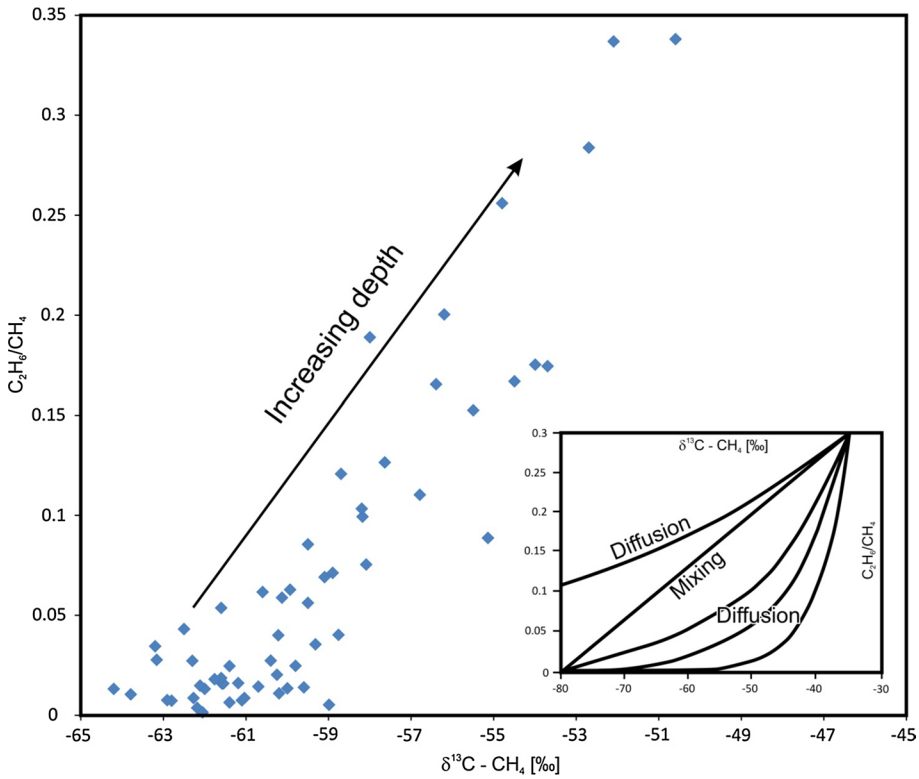

Fig. 11 Cross-plot of C_1/C_2 molecular ratio versus $\delta^{13}C$ of methane (after Prinzhofer and Pernaton 1997) of mudgas from a well near the southern margin of the Alpine Foreland Basin. Inset presents theoretical mixing and diffusion trends. Diffusion trends depend on ratios of the diffusive permeabilities for ethane over methane

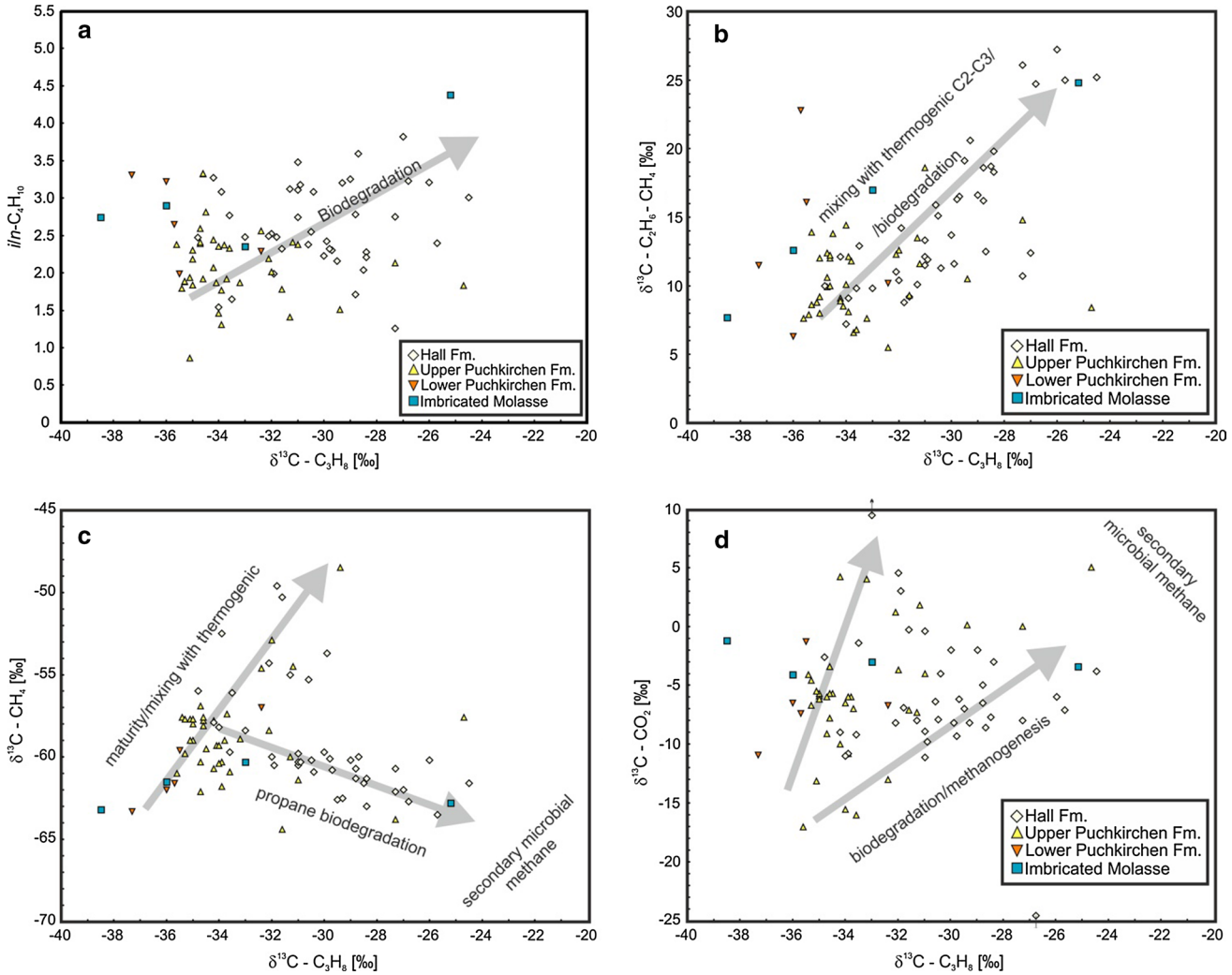

Fig. 12 Correlation of molecular and isotopic composition. *Gray arrows* indicate possible selective components removal and mixing with thermogenic hydrocarbons

isotopically methane enriched in ^{13}C (−48 to −61.4‰) testifying to a high amount of thermogenic gas are located both along the axis of the Puchkirchen Channel and above an area where more than 60 m of lower Oligocene fine-grained rocks have been removed by submarine erosion (Sachsenhofer and Schulz 2006). In contrast, the KK field hosting no thermogenic hydrocarbons, but pure microbial gas is located far north of the Puchkirchen Channel and in an area with thick pelitic Lower Oligocene deposits.

Migration through low-permeability caprocks may involve diffusion. Diffusion processes lead to molecular and isotopic fractionation due to differences in the effective diffusion coefficients (e.g., Krooss et al. 1988; Leythaeuser et al. 1983; Xia and Tang 2012; Zhang and Krooss 2001). Prinzhofer and Pernaton (1997) proposed a plot of the C_2/C_1 ratio versus $\delta^{13}C$ of methane (Fig. 11) to distinguish diffusive fractionation from simple mixing of two end-member gases. Because the Prinzhofer plot may be used for gases in seal rocks, but not for reservoir gases (Zhang and Krooss 2001) and because the thermogenic end-member gas in the case of the Alpine Foreland Basin is a gas mixture itself (Pytlak et al. 2016), we do not plot reservoir gas data, but mud gas data from a recently drilled well, which penetrated shaly units, several hundred meters thick. The mud gas data show a strong linear relationship between the C_2/C_1 ratio and $\delta^{13}C$ of methane (in the plot with linear axis) suggesting that mixing processes are dominant, whereas fractionation associated with diffusion does not appear to have influenced gas compositions significantly. Obviously, diffusive fractionation cannot be completely

ruled out, but its effect on the governing molecular and isotopic gas composition may have been overprinted by other processes (mixing, alteration; see below).

Gas biodegradation and secondary microbial methane

During microbial alteration of gaseous hydrocarbons propane is primarily degraded (Head et al. 2003; Kniemeyer et al. 2007). In addition, straight chain alkanes are preferentially removed compared to branched ones (James and Burns 1984; Palmer 1993) resulting in increasing *i*/*n*-C_4 ratios. Although *i*/*n*-C_4 ratio can depend on maturity (Alexander et al. 1981), those of non-degraded gases are usually below 0.8 (Huang and Larter 2014). In most cases microbial activity leads to enrichment in ^{13}C isotope of remaining molecules (e.g., C_3, *n*-C_4).

To visualize gas alteration trends, *i*/*n*-C_4 ratios and stable carbon isotopic composition of propane are plotted versus depth in Fig. 8c, d. *i*/*n*-C_4 ratios significantly above 0.8 indicate that all gases are biodegraded. *i*/*n*-C_4 ratios show a weak, $\delta^{13}C$ ratios of propane a strong downward decreasing trend providing evidence that the effect of in-reservoir biodegradation decreases downward with increasing formation temperature. Although microbes may be active at high temperatures, it is commonly accepted that microbial activity relevant for petroleum formation and degradation is restricted to temperatures below 80 °C (Head et al. 2003 and references therein). This observation agrees with the fact that in the study area a formation temperature of 80 °C is reached between 1500 and 2000 m depth subsea (Kamyar 2000). However, it is important to note that regional uplift after Late Miocene maximum burial resulted in cooling of about 20 °C (Gusterhuber et al. 2012). This argues for biodegradation, at least in deep reservoirs, before or after maximum burial.

The natural gas plot (Chung et al. 1988) shows that a significant number of samples show deviations from typical $\delta^{13}C$ distribution patterns ($\delta^{13}C_{C2H6} < \delta^{13}C_{C3H8} < \delta^{13}C_{C4H10}$; Schoell 1984; Tang et al. 2000) (Fig. 7b, d). This is caused mainly by an enrichment of ^{13}C in propane and reflects the selective microbial removal of this compound.

Some samples contain ethene and propene (Fig. 8), which are considered instable over geological timescales. Although microbial processes yielding unsaturated hydrocarbons are poorly understood, their presence may indicate recent bacterial activity (Whiticar 1994). Microbial activity is also confirmed by the presence of metabolites in reservoir rocks (Gruner, pers. comm.). Drill bit metamorphism as source for unsaturated hydrocarbons in reservoirs, which are in production since several years, can be ruled out. Whereas (ongoing) biodegradation is well confirmed, only a weak correlation is observed in the cross-plot of *i*/*n*-C_4 versus $\delta^{13}C$ of propane (Fig. 12a).

A general positive relation exists between the difference of $\delta^{13}C$ of methane and ethane and the $\delta^{13}C$ of propane (Fig. 12b). This may result from either gas mixing or biodegradation. A cross-plot of $\delta^{13}C$ of methane versus $\delta^{13}C$ of propane shows two separate trends indicative for mixing and biodegradation of propane, respectively (Fig. 12c).

Recently, biodegradation of hydrocarbons followed by methanogenesis has been recognized as a significant source of (secondary microbial) gas (e.g., Head et al. 2003; Jones et al. 2008; Milkov 2010; Zengler et al. 1999). The isotopic signature of secondary microbial methane depends on different factors, including the methanogenic community, reaction pathways, progress of alteration, isotopic signature of the substrate and reservoir temperature (Brown 2011; Jones et al. 2008). Frequently, secondary microbial methane is accompanied by CO_2 enriched in the ^{13}C isotope (up to 20‰) (Milkov 2011 and references therein). Methane depleted in ^{13}C (−65‰ or lower) is produced when CO_2 reduction commences, while CO_2 is moderately enriched in ^{13}C isotope (Jones et al. 2008). However, as CO_2 reduction progresses, carbon in both, CO_2 and methane, become heavier. CO_2 concentrations in total gas volume are not necessarily high, since CO_2 can be transformed into calcite cement (Dimitrakopoulos and Muehlenbachs 1987; Wiggins et al. 1993). Actually, Grundtner et al. (2014) could show that organic matter-derived CO_2 triggering calcite precipitation plays an important role in the diagenetic history of the Alpine Foreland Basin. In the present study measured $\delta^{13}C$ of CO_2 reaches values up to 18‰ with an average value of −5.9‰ (Table 1; Fig. 12d). Moreover, a general positive relation between $\delta^{13}C$ of CO_2 and C_3H_8 points to methanogenesis (Table 1; Fig. 12d). Therefore, biodegradation and formation of secondary microbial gas are considered at least as a minor additional source of methane.

Generation of secondary microbial methane results in gas drying. This may explain the relative high dryness values of gas samples with high $\delta^{13}C$ ratios.

Conclusions

Gas trapped in Oligocene–Miocene reservoir rocks in the Alpine Foreland Basin has traditionally been considered (primary) microbial in origin. A detailed investigation of samples from all producing gas fields provides a more differentiated picture, which contributes significantly to the understanding of the petroleum system.

- Dryness and the most negative $\delta^{13}C$ values of methane suggest a pure primary microbial origin of gas in Oligocene–Miocene reservoir horizons in the KK field, confirming the traditional model.

- In all others samples heavier hydrocarbons are present. The amount of C_{2+} hydrocarbons increases with reservoir depth, indicating a downward increasing contribution of thermogenic hydrocarbons. Varying contributions of thermogenic hydrocarbons are also reflected by strongly varying $\delta^{13}C$ values of methane. Based on $\delta^{13}C$ values of methane, gas from the F–O field in the western part of the study area contains the highest contribution of thermogenic hydrocarbons.
- The thermogenic hydrocarbons display an oil-window maturity and are derived from the deeper Mesozoic and Eocene oil-bearing reservoir and carrier beds. Upward migration along faults is likely (e.g., fields in the eastern part of the study area). Migration also occurred through low-permeability seal rocks (e.g., along subseismic fractures). Migration may have been facilitated in areas where lower Oligocene pelitic rocks are eroded and along the Puchkirchen Channel system, where a high percentage of permeable clastic rocks have been deposited. An effect of diffusion on molecular and isotopic composition of the gas cannot be observed.
- All gas samples in Oligocene–Miocene reservoirs are biodegraded, but the degree of biodegradation decreases downward. Biodegradation results in an increase in the i/nC_4 ratio, a selective removal of propane, an increase in $\delta^{13}C$ of propane and gas drying.
- Biodegradation is accompanied with the generation of secondary microbial methane (and ^{13}C enriched CO_2) resulting in further drying of the gas. Hence, gas dryness is high even in samples with high contributions of thermogenic hydrocarbons.
- The presence of alkenes suggests that biodegradation is an ongoing process.

Acknowledgements The presented data were obtained within the frame of FFG bridge Project 836527 between Montanuniversitaet Leoben and Rohöl-Aufsuchungs AG. The authors would like to thank Rohöl-Aufsuchungs AG for access to samples, geological documentation and publication permission. Fruitful discussion with Werner Tschelaut, Wilma Troiss, Alan Reingruber and Lorenz Scheucher (Rohöl-Aufsuchungs AG), Marie-Louise Grundtner (Montanuniversitaet Leoben), Andrea Gruner (GFZ German Research Centre for Geosciences), Heinz Wilkes (Oldenburg University) improved this paper. The article was improved considerably by review of Dr. Gabor C. Tari and anonymous reviewer.

References

Alexander R, Kagi RI, Woodhouse GW (1981) Variation in the ratio of isomeric butanes with sediment temperature in the carnarvon basin of Western Australia. In: Bjoroey M, Albrecht C, Cornford C, de Groot K, Eglinton G, Galimov E, Leythaeuser D, Pelet R, Rullkoetter J, Speers G (eds) Advances in organic geochemistry, 1981: proceedings of the international meeting on organic geochemistry, vol 10, pp 76–79

Belaed S (2007) Charakterisierung potenzieller Muttergesteine für biogenes Erdgas in der österreichischen Molassezone. Diploma thesis. Technical University of Clausthal, Germany

Bernard BB, Brooks JM, Sackett WM (1978) Light hydrocarbons in recent Texas continental shelf and slope sediments. J Geophys Res 83:4053–4061

Berner U, Faber E (1987) Maturity related mixing model for methane, ethane and propane, based on carbon isotopes. Org Geochem 13:67–72

Berner U, Faber E (1996) Empirical carbon isotope/maturity relationships for gases from algal kerogens and terrigenous organic matter, based on dry, open-system pyrolysis. Org Geochem 24:947–955

Brix F, Schultz O (1993) Erdöl und Erdgas in Österreich, 2nd edn. Veröffentlichungen aus dem Naturhistorischen, Wien

Brown A (2011) Identification of source carbon for microbial methane in unconventional gas reservoirs. AAPG Bull 95:1321–1338

Chung HM, Gormly JR, Squires RM (1988) Origin of gaseous hydrocarbons in subsurface environments: theoretical considerations of carbon isotope distribution. Chem Geol 71:97–104

Clayton C (1991) Carbon isotope fractionation during natural gas generation from kerogen. Mar Pet Geol 8:232–240

Covault JA, Hubbard SM, Graham SA, Hinsch R, Linzer H (2009) Turbidite-reservoir architecture in complex foredeep-margin and wedge-top depocenters, Tertiary Molasse foreland basin system, Austria. Mar Pet Geol 26:379–396

Dai J (1990) Characteristics of hydrogen isotopes of paraffinic gas in China. Pet Explor Dev 17:27–32

Dimitrakopoulos R, Muehlenbachs K (1987) Biodegradation of petroleum as a source of ^{13}C-enriched carbon dioxide in the formation of carbonate cement. Chem Geol 65:283–291

Fuex AN (1977) The use of stable carbon isotopes in hydrocarbon exploration. J Geochem Explor 7:155–188

Galimov EM (2006) Isotope organic geochemistry. Org Geochem 37:1200–1262

Grundtner M-L, Pytlak L, Gross D, Linzer H.-G, Sachsenhofer RF (2014) Rock-fluid interactions in reservoir rocks of the Molasse Basin. In: EMAS 2014—11th regional workshop on electron probe microanalysis today—practical aspects, Leoben

Grunert P, Hinsch R, Sachsenhofer RF, Bechtel A, Ćorić S, Harzhauser M, Piller W, Sperl H (2013) Early Burdigalian infill of the Puchkirchen Trough (North Alpine Foreland Basin, Central Paratethys): facies development and sequence stratigraphy. Mar Pet Geol 39:164–186

Grunert P, Auer G, Harzhauser M, Piller WE (2015) Stratigraphic constraints for the upper Oligocene to lower Miocene Puchkirchen Group (North Alpine Foreland Basin, Central Paratethys). Newsl Stratigr 48:111–133

Gusterhuber J, Dunkl I, Hinsch R, Linzer H-G, Sachsenhofer RF (2012) Neogene uplift and erosion in the Alpine Foreland Basin (Upper Austria and Salzburg). Geol Carpath 63:295–305

Gusterhuber J, Hinsch R, Linzer H-G, Sachsenhofer R (2013) Hydrocarbon generation and migration from sub-thrust source rocks to foreland reservoirs: the Austrian Molasse Basin. Austrian J Earth Sci 106:115–136

Head IM, Jones DM, Larter SR (2003) Biological activity in the deep subsurface and the origin of heavy oil. Nature 426:344–352

Hinrichs K-U, Hayes JM, Bach W, Spivack AJ, Hmelo LR, Holm NG, Johnson CG, Sylva S (2006) Biological formation of ethane and propane in the deep marine subsurface. Proc Natl Acad Sci USA 103:14684–14689

Hoering TC (1984) Thermal reactions of kerogen with added water, heavy water and pure organic substances. Org Geochem 5:267–278

Huang H, Larter S (2014) Secondary microbial gas formation associated with biodegraded oils from the Liaohe Basin, NE China. Org Geochem 68:39–50

Hubbard SM, De Ruig MJ, Graham SA (2005) Utilizing outcrop analogs to improve subsurface mapping of natural gas-bearing strata in the Puchkirchen Formation, Molasse Basin, Upper Austria. Austrian J Earth Sci 98:52–66

Hubbard SM, De Ruig MJ, Graham S (2009) Confined channel-levee complex development in an elongate depo-center: deep-water Tertiary strata of the Austria Molasse basin. Mar Pet Geol 26:85–112

James AT (1983) Correlation of natural gas by use of carbon isotopic distribution between hydrocarbon components. AAPG Bull 67:1176–1191

James AT (1990) Correlation of reservoired gases using the carbon isotopic compositions of wet gas components. AAPG Bull 74:1441–1458

James AT, Burns BJ (1984) Microbial alteration of subsurface natural gas accumulations. AAPG Bull 68:957–960

Jones DM, Head IM, Gray ND, Adams JJ, Rowan AK, Aitken CM, Bennett B, Huang H, Brown A, Bowler BFJ, Oldenburg T, Erdmann M, Larter SR (2008) Crude-oil biodegradation via methanogenesis in subsurface petroleum reservoirs. Nature 451:176–181

Kamyar HR (2000) Verteilung der Untergrundstemperaturen an den Beispielen der Bohrlochtemperatur (BHT)—Messungen in den RAG—Konzessionen Oberösterreichs und Salzburgs, (Molasse- und Flyschzone). Ph.D. thesis, University of Vienna, Austria

Kniemeyer O, Musat F, Sievert S, Knittel K, Wilkes H, Blumenberg M, Michaelis W, Classen A, Bolm C, Joye S, Widdel F (2007) Anaerobic oxidation of short-chain hydrocarbons by marine sulfate-reducing bacteria. Nature 449:898–901

Krooss BM, Leythaeuser D, Schaefer RG (1988) Light hydrocarbon diffusion in a caprock. Chem Geol 71:65–76

Krooss BM, Littke R, Miiller B, Frielingsdorf J, Schwochau K, Idiz EF (1995) Generation of nitrogen and methane from sedimentary organic matter: implications on the dynamics of natural gas accumulations. Chem Geol 126:291–318

Lewan MD (1993) Laboratory Simulation of Petroleum Formation. In: Engel MH, Macko SA (eds) Organic geochemistry-principles and applications. Plenum Press, New York, pp 419–422

Lewan MD (1997) Experiments on the role of water in petroleum formation. Geochim Cosmochim Acta 61:3691–3723

Leythaeuser D, Schaefer RG, Pooch H (1983) Diffusion of light hydrocarbons in subsurface sedimentary rocks. AAPG Bull 67:889–895

Littke R, Krooss BM, ldiz E, Frielingsdorf J (1995) Molecular nitrogen in natural gas accumulations: generation from sedimentary organic matter at high temperatures. AAPG Bull 79:410–430

Malzer O, Rögl F, Seifert P, Wagner L, Wessely G, Brix F (1993) Muttergesteine, speichergesteine, migration und lagerstättenbildung in der molassezone und deren sedimentärem untergrund. In: Brix F, Schultz O (eds) Erdöl und Erdgas in Österreich, 2 Auflage, Wien, pp 302–315

Masalimova LU, Lowe DR, McHargue T, Derksen R (2015) Interplay between an axial channel belt, slope gullies and overbank deposition in the Puchkirchen Formation in the Molasse Basin, Austria. Sedimentology 62:1717–1748

Milkov AV (2010) Methanogenic biodegradation of petroleum in the West Siberian Basin (Russia): significance for formation of giant Cenomanian gas pools. AAPG Bull 94:1485–1541

Milkov AV (2011) Worldwide distribution and significance of secondary microbial methane formed during petroleum biodegradation in conventional reservoirs. Org Geochem 42:184–207

Ni Y, Ma Q, Ellis GS, Dai J, Katz B, Zhang S, Tang Y (2011) Fundamental studies on kinetic isotope effect (KIE) of hydrogen isotope fractionation in natural gas systems. Geochim Cosmochim Acta 75:2696–2707

Oremland RS, Whiticar MJ, Strohmaier FE, Kiene RP (1988) Bacterial ethane formation from reduced, ethylated sulfur compounds in anoxic sediments. Geochim Cosmochim Acta 52:1895–1904

Palmer SE (1993) Effect of biodegradation and water washing on crude oil composition. In: Engel MH, Macko SA (eds) Organic geochemistry. Plenum Press, New York, pp 511–533

Prinzhofer A, Pernaton É (1997) Isotopically light methane in natural gas: bacterial imprint or diffusive fractionation? Chem Geol 142:193–200

Pytlak L, Gross D, Bechtel A, Gratzer R, Sachsenhofer RF, Linzer H-G, Grundtner M-L, Scheucher L (2014) Origin and alteration of natural gas and liquid hydrocarbons accumulated in the Austrian molasse basin. In: AAPG international conference and exhibition, Sept 16th, Istanbul, Turkey

Pytlak L, Gross D, Sachsenhofer RF, Bechtel A, Gratzer R, Linzer H-G (2016) Generation, mixing and alteration of thermogenic and microbial gas in oil deposits: the case of the Alpine Foreland Basin (Austria). Mar Pet Geol 78:575–592

Radke J, Bechtel A, Gaupp R, Püttmann W, Schwark L, Sachse D, Gleixner G (2005) Correlation between hydrogen isotope ratios of lipid biomarkers and sediment maturity. Geochim Cosmochim Acta 69:5517–5530

Reischenbacher D, Sachsenhofer RF (2011) Entstehung von Erdgas in der oberosterreichischen Molassezone: daten und offene Fragen. Berg- und Huttenmannische Monatshefte 156:463–468

Rice DD, Claypool GE (1981) Generation accumulation, and resource potential of biogenic gas. AAPG Bull 65:5–25

Rooney MA, Claypool GE, Chung HM (1995) Modeling thermogenic gas generation using carbon isotope ratios of natural gas hydrocarbons. Chem Geol 126:219–232

Sachsenhofer RF, Schulz H-M (2006) Architecture of Lower Oligocene source rocks in the Alpine Foreland Basin: a model for syn- and post-depositional source-rock features in the Paratethyan realm. Pet Geosci 12:363–377

Sachsenhofer RF, Leitner B, Linzer H-G, Bechtel A, Coric S, Gratzer R, Reischenbacher D, Soliman A (2010) Deposition, erosion and hydrocarbon source potential of the oligocene eggerding formation (Molasse Basin, Austria). Austrian J Earth Sci 103:76–99

Schimmelmann A, Boudou J-P, Lewan MD, Wintsch RP (2001) Experimental controls on D/H and $^{13}C/^{12}C$ ratios of kerogen, bitumen and oil during hydrous pyrolysis. Org Geochem 32:1009–1018

Schimmelmann A, Sessions AL, Boreham CJ, Edwards DS, Logan GA, Summons RE (2004) D/H ratios in terrestrially sourced petroleum systems. Org Geochem 35:1169–1195

Schoell M (1977) Die Erdgase der süddeutschen Molasse—Anwendung von D/H- und ^{13}C-/^{12}C Isotopenanalysen zur Klärung ihrer Entstehung. Erdöl Erdgas Z 93:311–322

Schoell M (1980) The hydrogen and carbon isotopic composition of methane from natural gases of various origins. Geochim Cosmochim Acta 44:649–661

Schoell M (1983) Genetic characterization of natural gases. AAPG Bull 67:2225–2238

Schoell M (1984) Wasserstoff und kohlenstoffisotope in organischen substanzen. Erdolen und Erdgasen. Geol Jahrb Reihe D 67, Bundesanstalt für Geowissenschaften und Rohstoffe, Hannover

Schulz H-M, van Berk W (2009) Bacterial methane in the Atzbach-Schwanenstadt gas field (upper Austrian Molasse Basin), Part II: retracing gas generation and filling history by mass balancing of organic carbon conversion applying hydrogeochemical modelling. Mar Pet Geol 26:1180–1189

Schulz H-M, Sachsenhofer RF, Bechtel A, Polesny H, Wagner L (2002) The origin of hydrocarbon source rocks in the Austrian Molasse Basin. Mar Pet Geol 19:683–709

Seewald JS, Benitez-Nelson B, Whelan JK (1998) Laboratory and theoretical constrains on the generation and composition of natural gas. Geochim Cosmochim Acta 62:1599–1617

Sessions AL, Sylva SP, Summons RE, Hayes JM (2004) Isotopic exchange of carbon-bound hydrogen over geologic timescales. Geochim Cosmochim Acta 68:1545–1559

Stahl WJ (1977) Carbon and nitrogen isotopes in hydrocarbon research and exploration. Chem Geol 20:121–149

Tang Y, Perry JK, Jenden PD, Schoell M (2000) Mathematical modeling of stable carbon isotope ratios in natural gases. Geochim Cosmochim Acta 64:2673–2687

Tang Y, Huang Y, Ellis GS, Wang Y, Kralert PG, Gillaizeau B, Ma Q, Hwang R (2005) A kinetic model for thermally induced hydrogen and carbon isotope fractionation of individual *n*-alkanes in crude oil. Geochim Cosmochim Acta 69:4505–4520

Veron J (2005) The Alpine Molasse Basin—review of petroleum geology and remaining potential. Bull Angew Geol 10:75–86

Wagner LR (1996) Stratigraphy and hydrocarbons in upper Austrian Molasse Foredeep (active margin). In: Wessely G, Liebl W (eds) Oil and gas in alpidic thrust belts and Basins of Central and Eastern Europe, vol 5. European Association of Geoscientists and Engineers Special Publication, London, pp 217–235

Wagner LR (1998) Tectono-stratigraphy and hydrocarbons in the Molasse Foredeep of Salzburg, upper and lower Austria. In: Mascle A, Puigdefabregas C, Luterbacher HP, Fernandez M (eds) Cenozoic foreland basins of Western Europe, vol 134. Geological Society Special Publications, London, pp 339–369

Whiticar MJ (1994) Correlation of natural gases with their sources. In: Magoon LB, Dow WG (eds) The petroleum system—from source to trap, vol 60. AAPG Memoir, Tulsa, pp 261–283

Whiticar MJ, Suess E (1990) Hydrothermal hydrocarbon gases in the sediments of the King George Basin, Bransfield Strait, Antarctica. Appl Geochem 5:135–147

Whiticar MJ, Faber E, Scheoll M (1986) Microbial methane formation in marine and freshwater environments: carbon dioxide reduction vs. acetate fermentation—isotope evidence. Geochim Cosmochim Acta 50:693–709

Wiggins WD, Harris PM, Burruss RC (1993) Geochemistry of post-uplift calcite in the Permian Basin of Texas and New Mexico. Geol Soc Am Bull 105:779–790

Xia X, Tang Y (2012) Isotope fractionation of methane during natural gas flow with coupled diffusion and adsorption/desorption. Geochim Cosmochim Acta 77:489–503

Yoneyama Y, Okamura M, Morinaga K, Tsubaki N (2002) Role of water in hydrogenation of coal without catalyst assition. Energy Fuel 16:48–53

Zengler K, Richnow HH, Rossello-Mora R, Michaells W, Widdel F (1999) Methane formation from long-chain alkanes by anaerobic microorganisms. Nature 401:266–269

Zhang T, Krooss BM (2001) Experimental investigation on the carbon isotope fractionation of methane during gas migration by diffusion through sedimentary rocks at elevated temperature and pressure. Geochim Cosmochim Acta 65:2723–2742